Design and validation of a mobile laboratory for testing air inlet filter loading at animal houses

Benjamin C. Smith[1], Brett C. Ramirez[1*], Steven J. Hoff[1],
Jay D. Harmon[1], John P. Stinn[1]

(1. *Department of Agricultural and Biosystems Engineering, Iowa State University, Ames, IA USA*;
2. *Iowa Select Farms, Iowa Falls, IA USA*)

Abstract: The US swine industry is shifting towards filtered fresh-air ventilation systems that use pleated filters to improve breeding herd health and reduce airborne disease outbreak frequency. Loaded filters reduce airflow causing a poor environment and elevated energy use. Typical axial fans cannot efficiently maintain the rated differential pressure (DP; 100 Pa) for pleated filters; hence, a lower design filter DP (37 Pa) is used and consequently, more filters are required to achieve design maximum ventilation. Large, common filter banks for multiple staged fans present significant challenges in using continuous DP measurement to assess filter life, making it impossible to separate filter loading DP from overall airflow DP. A mobile air filter testing (MAFT) laboratory is needed to provide timely farm-to-farm testing of on-site filters by accurately measuring airflow at given DPs to identify filter end-of-life and enable research on spatiotemporal filter loading characteristics. The MAFT laboratory consisted of a 4.6 m long acrylic test duct mounted in an enclosed trailer capable of operating at 37 Pa DP across primary and secondary filter combinations for 169 to 1,692 m^3 hr^{-1} airflows. Test duct calibration (R^2>0.99; RMSE=8.40×10 m^3 hr^{-1}) at BESS Labs and validation against an off-site third-party laboratory (34 loaded filters from commercial swine facilities) showed good agreement (p<0.0001). Relative expanded uncertainty was calculated to range from 1.5% to 5% (1,417 to 343 m^3 hr^{-1}). The MAFT laboratory provides a unique approach for testing agricultural filter performance directly on-farm to eliminate the time and cost to test filters off-site at third-party laboratories.

Keywords: biosecurity, disease transmission, PRRS virus, swine, ventilation

Citation: Smith, B. C., B. C. Ramirez, S. J. Hoff, J. D. Harmon, and J. P. Stinn. 2019. Design and validation of a mobile laboratory for testing air inlet filter loading at animal houses. Agricultural Engineering International: CIGR Journal, 21(3): 39–50.

1 Introduction

The demand for food production, specifically animal-based protein, will increase with the concurrent world population growth (Thornton, 2010); hence, an increased efficiency in swine production is needed to meet this intensifying demand. The US swine industry currently faces numerous challenges inhibiting production efficiency, such as herd health, heat stress, management, etc. Improvement of biosecurity practices can reduce the frequency of disease outbreaks in the sow herd resulting in lower pre-wean mortality and higher overall herd health. Porcine Reproductive and Respiratory Syndrome Virus (PRRSV) is an airborne disease effecting both sow and finishing herds and has the largest negative economic impact on the US swine industry at an estimated average of 664 USD million per year (Holtkamp et al., 2013). Therefore, a decrease in disease transmission via routes that are commonly and previously overlooked is needed to sustain economic and efficient production of animal-based protein.

Industry efforts have focused on identifying and addressing the major routes of disease transmission into swine facilities; however, airborne routes are typically excluded (Ramirez and Zaabel, 2012). Filtration of the fresh air ventilation can control airborne disease transmission and has been shown to have potential

Received date: 2018-10-17 **Accepted date:** 2019-02-22

*** Corresponding author: Brett C. Ramirez**, Ph.D., Assistant Professor, Iowa State University, Department of Agricultural and Biosystems Engineering, 4348 Elings Hall, Ames, Iowa 50011 USA. Ph: +001-515-294-0468, Email: bramirez@iastate.edu.

long-term economic impact (Alonso et al., 2013a; Dee et al., 2010). Since the adoption of filtration, production of PRRS negative pigs has increased from 59% (pre-filtration) to 93% (post-filtration) with an accompanying increased economic value estimated at 5 USD per pig weaned (Alonso et al., 2013a). In the Midwest, air filtration is most commonly utilized on breeding-gestation-farrowing buildings. Air filters can be installed in a variety of locations depending on the ventilation system style. For traditional negative pressure ventilation systems, air filters are commonly installed directly above the existing ceiling air inlet system (located in the attic space) to filter air entering through ceiling inlets, or alternatively, in a filter wall at the inlet to tunnel ventilation (Alonso et al., 2013b). A potential drawback of implementing filters in a negative pressure system is un-filtered air can enter the room through building envelope infiltration (Jadhav et al., 2018). An alternative approach is a positive pressure ventilation system. Fresh air can be either pulled or pushed through filters to ultimately achieve a slightly positive pressure in the attic and occupied pig space, relative to outside conditions(Ramirez et al., 2016). The main advantage of positive pressure ventilation is the prevention of un-filtered infiltration into the filtered air spaces (Albright, 1990). Both types of ventilation systems use similar components, such as, axial fans, actuated inlets, shutters, filters, evaporative pads, etc. to achieve a filtered airspace. Two types of filter categories (primary then secondary) are commonly used in series in these ventilation systems: pleated primary (Minimum Efficiency Reporting Value, MERV 4 to 8) and pleated secondary filters (MERV 14 to 16) (Dee et al., 2006). Unlike traditional Heating, Ventilation, and Air Conditioning (HVAC) systems where primary and secondary filters have a separation distance (e.g., >0.5 m), in animal agriculture applications, the primary filter is mounted directly to the face of the secondary filter.

Axial fans, designed for high volume, low pressure applications (i.e., animal housing filtration), are most energy efficient at a maximum operating static differential pressure (DP) of 75 Pa (University of Illinois, 2012). Given a design DP of ~13 Pa across an evaporative pad and a desired DP of ~25 Pa across common ceiling inlet systems, a maximum 37 Pa operating DP is desired across the combined primary and secondary filter bank assembly. This 37 Pa DP is much less than the typical filter manufacturer's minimum rated operating DP of 100 Pa (McQuiston et al., 2005). For filters operated at lower than the manufacturer's rated value, filter efficiency can be negatively impacted because face velocity is insufficient for filtration mechanisms (which are mainly based on impaction) to function correctly. An additional consequence is, the airflow per single filter pair (a pair is the combination of a prim. and a sec. filter) is less than the manufacturer's rated airflow (McQuiston et al., 2005). The combined effect of the 37 Pa design DP and range of design airflows in animal housing results in unique implications for ventilation system design. For example, at maximum summertime design ventilation rates (850 $m^3 hr^{-1}$ per sow and litter and 510 $m^3 hr^{-1}$ per gestating sow), a 4,000 head (3,200 sows and 800 sows and litters) breeding-gestation-farrowing site with six buildings (a common commercial site layout) would require a total of 2,132 filter pairs based on typical air filter design data (1,084 $m^3 hr^{-1}$ per filter) at a DP of 37 Pa (McQuiston et al., 2005; Midwest Plan Service, 2010). In contrast, for the same maximum summertime ventilation rate, a total of 800 filters is needed in a HVAC system for human-occupied buildings operating at the filter manufacturer's rated operating condition (2,889 $m^3 hr^{-1}$ at DP=100 Pa) (McQuiston et al., 2005).

Effective filter operation in a ventilation system can be ensured by routine filter performance testing for filter efficiency and filter resistance. Filter efficiency is reported as the MERV on a scale of: MERV 1 (lowest efficiency) to MERV 16 (highest efficiency) (ASHRAE Standard, 2012). Filter resistance is defined as the DP across a filter pair at a given airflow. The ASHRAE 52.2-2012 standard states the test duct parameters and methodology to perform filter performance tests as a function of particle size. For a filter resistance test, a variable speed blower or damper adjusts airflow (at >100 Pa DP across a long radius nozzle) through an ASHRAE 52.2 certified test duct to achieve a desired DP across the filter pair; however, at low airflows and DPs, measurement uncertainty tends to increase because

measurements occur near the minimum of the full-scale (FS) transducer range (accuracy is often stated at the maximum FS value). Results obtained from testing a sample of filter pairs from a ventilation system could be used to indicate if all filter pairs need to be replaced. Filter resistance testing may need to occur frequently (approximately three times per year) due to dust loading causing an increase in DP and reduction in airflow. Levels of dust loading depends on conditions adjacent to the filtered site, such as, row crop operations, livestock and poultry facility particulate emissions, unpaved roads, and grain handling facilities. The cost associated with shipping and testing filter pairs at an off-site third-party laboratory can be prohibitive if a large number of filters is needed to make improved management decisions for filter replacement.

An *in situ* monitoring system for monitoring filter resistance and airflow, would require the pressure differential across the filters and across the fans to be monitored, as well as fan power consumption. Since inlet air filters are installed in either large common filter banks with multiple fans or over all ceiling inlets, monitoring pressure drop quickly becomes a technical challenge. The variable airflow system used in animal houses also complicates *in situ*, with all filters being used at every airflow rate. Furthermore, this method would require a fan calibration to calculate a pressure differential and airflow relationship for the filters required to interpret the filter pressure difference correctly. Fan calibrations and continuous monitoring are challenging because of biosecurity, logistical concerns, and sensor longevity. These concerns make an *in situ* monitoring system an impractical option to implement for improving a filter management system.

A mobile air filter testing (MAFT) laboratory capable of on-site testing of just filter resistance (airflow at a design pressure difference) at the design DP of 37 Pa accompanied with a documented statement of measurement uncertainty is needed to reduce the cost associated with filter testing off-site at third-party laboratories and provide information for improved management decisions. The intended application of the MAFT laboratory is to travel to rural swine facilities and test a representative sample of both primary and secondary filter pairs. Further, the test results will include a quantified standard uncertainty associated with final airflow prediction for confidence and improved reliability – comparable to an off-site third-party laboratory. Both time and expenses can be substantially reduced with a mobile laboratory by eliminating filter shipping and decreasing the overall time from sampling to receiving test results. The implementation of MAFT allows for tested filters to be reinstalled because the testing occurred on-site and biosecurity protocols can be adhered to. When only a primary filter is tested, the secondary filter can remain installed. For testing a secondary filter, the secondary filter is replaced temporarily with a new secondary filter or a cap to prevent un-filtered air from entering the building, as opposed to always replacing both filters when soliciting an off-site third-party certified laboratory. Additionally, the same filters can be tested over time to generate an accurate airflow reduction relationship to predict filter end-of-life as a function of pressure difference. The objectives of this study were: (1) to design and construct the MAFT laboratory to be housed in an enclosed trailer and to replicate design filter DP and face velocities; (2) to perform a detailed uncertainty analysis associated with predicted airflow by MAFT; and (3) to compare MAFT laboratory airflow predictions with an off-site third-party laboratory from field loaded filters to verify and validate MAFT application.

2 Materials and methods

The intended conceptual operation of the MAFT laboratory was to be self-sufficient – this includes, transportation to a site, setup of generator, instrumentation and equipment, collection of field loaded filters (i.e., filters that have been used in a commercial facility) to achieve a representative sample, performance of filter resistance tests, and finally, if needed, re-installation of those filters. The design criteria were to measure airflows expected for a filter pair (primary and secondary) at 37 Pa (0.15 in. wc) DP, have the overall test duct fit within an enclosed trailer with a maximum length of 9.7 m (32 ft), and adhere to the ASHRAE 52.2 standard specifications for test duct design, where applicable. A designed airflow range of 169 to 1,692

$m^3\ hr^{-1}$ (100 to 1,000 $ft^3\ min^{-1}$) at a filter surface area of 0.37 m^2 was selected based on the airflows typically experienced by filter pairs currently utilized in the swine industry. In addition, instrumentation was selected to minimize uncertainty in airflow predictions.

2.1 Design

The test duct was 4.57 m (15 ft) long and partitioned into four sections (length): entry (1.83 m; 6 ft), primary and secondary filter pair, nozzle upstream (1.52 m; 5 ft), and exhaust (1.22 m; 4 ft). Total length was constrained by the enclosed trailer length (Figure 1 and Table 1). Location of static pressure taps and cross-sectional area (Table 1) of the test duct were specified from ASHRAE Standard 52.2-2012 (2012). Although a variety of filter dimensions exist, the most common filter pairs used in the swine industry are 0.61×0.61 m (2×2 ft) and the standard specifies transitions to accommodate different sizes (ASHRAE Standard, 2012). A 2.24 kW (3 HP) radial blower (Model 7AT98, Dayton Manufacturing Co.) was sized to provide the design airflow range for the test duct. Airflow measurement per ASHRAE 52.2 requirements, was performed by a long radius nozzle selected for a maximum 373 Pa DP (1.5 in. wc) at 1,692 $m^3\ hr^{-1}$ (1,000 $ft^3\ min^{-1}$). A 15 kW split-phase generator (Model 5734, Generac, Inc.) was sized to meet all power demands and enable to MAFT laboratory to be standalone.

Table 1 Descriptions and dimensions for labels defined in Figure 1

Label	Description	Dimension
A	Test duct cross-sectional width and height	0.61 m (24 in.)
B	Exhaust section length	1.22 m (48 in.)
C	Long radius nozzle diameter	0.15 m (6 in.)
D	Nozzle face to pitot tube	0.31 m (12 in.)
E	Nozzle upstream section length	1.52 m (60 in.)
F	Filter downstream pitot tube	0.66 m (26 in.)
G	Pre-filter (primary) face to front of filter section	0.05 m (2 in.)
H	Filter section length	0.61 m (24 in.)
I	Entry section end to filter upstream pitot tube	0.25 m (10 in.)
J	Entry section length	1.83 m (72 in.)
K	Flow straightener hydraulic diameter	0.05 m (2 in.)
L	Flow straightener hydraulic length	0.31 m (12 in.)
M	Square duct to supply pipe transition length	0.32 m (25 in.)
N	Temperature probe placement in PVC pipe	0.10 m (4 in.)
O	PVC pipe length	0.36 m (14 in.)
P	Temperature probe placement length to end of pipe	0.20 m (8 in.)
Q	PVC pipe diameter	0.20 m (8 in.)

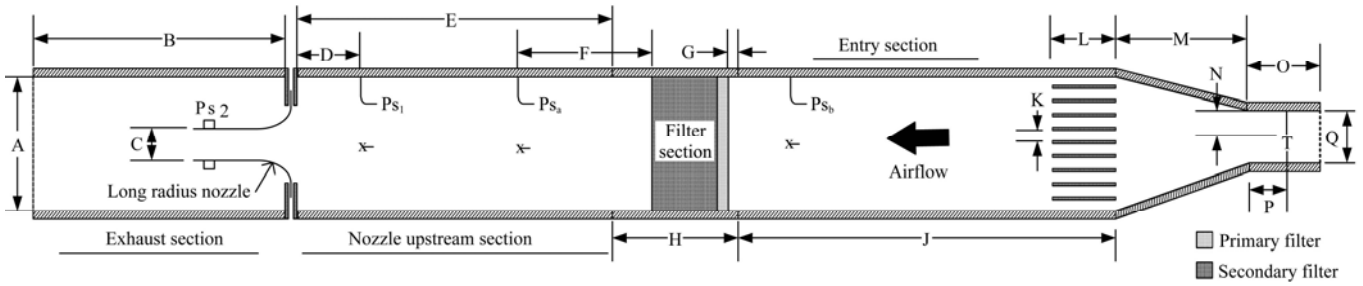

Figure 1 Test duct component design with labels A through Q defined in Table 1

The static pressure at each measurement location (Ps_a, Ps_b, Ps_1) was determined from the average of three static-only pitot tubes (top and both sides of the test duct). Filter assembly lengths were arbitrary to test duct length.

2.2 Construction

The test duct was housed in an enclosed trailer (Cross Trailers) with interior dimensions (L×W×H) of 7.3×2.6×2.13 m (24×8.5×7 ft) and retrofitted with a custom wiring setup to accommodate the AC circuits for blower, air conditioner, baseboard heaters, and instrumentation. A pleated filter inlet placed inside and at the front of the trailer was connected to the blower with a 4.9 m (16 ft) section of 0.2 m (8 in.) diameter flexible, insulated duct. The blower was placed inside a custom weatherproof housing that allowed access to the damper used for airflow control. The outlet of the blower was connected to the damper, which was then connected to a 1.52 m (5 ft) long flexible, insulated duct, with its outlet attached to a pipe fitted through the front of the trailer and ultimately then to the entry section of the test duct (Figure 2).

An entry transition was permanently secured to the trailer with the upstream opening attached to the supply pipe and the downstream opening secured to the entry section of the test duct. The entry transition consisted of a 0.2 m (8 in.) diameter to 0.31 m (12 in.) square duct boot inlet projected to 0.61 m (24 in.) square duct outlet with acrylic sides. The entry section was secured permanently in place, with the bottom of the duct located 0.61 m

(24 in.) above the trailer floor. A flow straightener was constructed by assembling a 10×10 lattice grid structure of 0.05 m (2 in.) diameter Schedule 80 PVC pipe. The filter section, nozzle upstream section, and exhaust section were placed on casters, which fit into a railing system built out of angle iron with dimensions (L×W×T) of 38×38×4.64 mm (1.5×1.5×0.18 in.) to allow forward and backward movement.

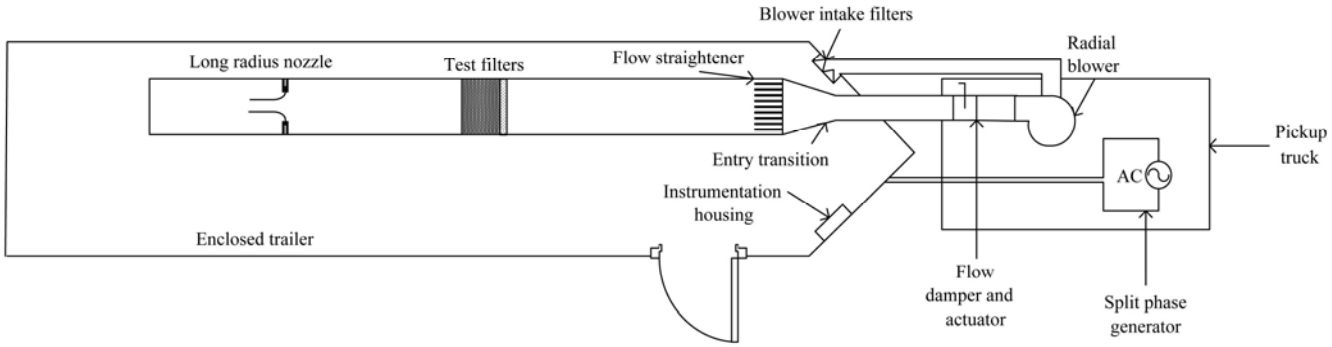

Figure 2 Overall schematic showing with MAFT housed inside an enclosed trailer with external radial blower and generator

The test duct walls were made of 6.35 mm (0.25 in.) thick clear acrylic and secured to an angle iron frame with dimensions (L×W×T) of 38×38×4.64 mm (1.5×1.5×0.18 in.) for support and rigidity. The acrylic and frame joints were sealed with silicone and the four test duct sections were bolted together with a foam strip gasket between them. The long radius nozzle (Helander Metal Spinning) was placed between two pieces of sheet metal, each with 0.36 m (14 in.) diameter holes at the centre to create a custom flange. The flange was bolted together with foam stripping placed along the holes to seal between the nozzle and the sheet metal pieces. In addition, the flange was then secured between the nozzle upstream and exhaust sections using bolts.

2.3 Instrumentation

An instrumentation system was developed to measure and record all necessary parameters needed for accurate airflow calculations, and to perform simple control of the equipment for filter resistance testing. Barometric pressure (Pb; Model 276, Setra Systems, Inc.) was measured inside the trailer and a combination dry-bulb temperature (t_{db}) and relative humidity (RH) probe (Model HMP-110, Vaisala) with a duct mounting attachment was placed in the supply pipe upstream of the entry transition. Two differential pressure transducers (DPTs; Model 267, Setra Systems, Inc.), designated as DPT_1 (0 to 248 Pa) and DPT_2 (0 to 373.2 Pa), were used to measure the static DP across the long radius nozzle (Ps_1 - Ps_2; Figure 1) and encompass the desired testing range, minimize uncertainty, and provide redundancy of measurements, and detect transducer malfunction. Upstream static pressure (Ps_1) was measured by averaging the static pressure from three static-only pitot tubes (Model A-302, Dwyer Instruments, Inc.) placed 0.31 m (12 in.) upstream of the long radius nozzle, while downstream static pressure (Ps_2) was measured using the average of four static throat taps in the long radius nozzle (Figure 1). A gas multiplexer made of a solenoid array controlled switching and isolated DPT_1 when the upstream and downstream static DP across the nozzle approached and exceeded 248 Pa. An additional DPT (DPT_3; 0 to 124 Pa; Model 267, Setra Systems, Inc) measured DP across the filters (Ps_a - Ps_b; Figure 1) from a set of three static only pitot tubes (Model A-302, Dwyer Instruments, Inc.) placed 0.31 m (12 in.) upstream and 0.66 m (26 in.) downstream from the face of the filters. An actuated damper (Model M9108-GGA, Johnson Controls) with 0 to10 VDC input was selected to control airflow on the downstream end of the radial blower. Analog voltages from all the transducers were measured as a differential input into a 16-bit data acquisition (DAQ) system (Model 16082AO, Measurement Computing, Inc.). Further, DPTs, solenoids, and power supplies were contained in a custom housing.

2.4 Operation

A custom program and graphical user interface were created in the development environment for visual basic for applications (VBA) to control the damper and collect data. A proportional-integral loop controlled airflow by adjusting damper opening area from static pressure feedback to achieve the desired DP across the filter. Once the desired filter DP and steady-state conditions were

achieved, data from all transducers were recorded for 15 s at 4 Hz and then averaged to calculate predicted airflow. If the long radius nozzle DP exceeded the threshold for either DPT_1 or DPT_2, the appropriate solenoids isolated and relieved the pressure to prevent damage to the transducer. For DP <248 Pa, both DPT_1 and DPT_2 were used (259 to 1,189 $m^3\ hr^{-1}$; 150 to 700 $ft^3\ min^{-1}$) and for DP >248 Pa, DPT_2 was used (259 to 1692 $m^3\ hr^{-1}$; 700 to 1,000 $ft^3\ min^{-1}$). Airflow calculations <1,189 $m^3\ hr^{-1}$ were performed by using the average DP of both DPT_1 and DPT_2.

The VBA program calculated airflow through the nozzle, assuming all mass was conserved, corrected the value to a standard airflow, and applied the calibration equation. Airflow calculations (ASHRAE, 2013; Equation (1)) were performed using the average t_{db}, RH, P_b, and nozzle DP (Equation (1)).

$$Q' = C_d \left(\frac{\pi d^2}{4} \right) \sqrt{\frac{2(Ps_1 - Ps_2)}{\rho(1-\beta^4)}} \quad (1)$$

where, Q' = predicted airflow ($m^3\ s^{-1}$); C_d = discharge coefficient (0.98); d = nozzle diameter (0.15 m); (Ps_1– Ps_2) = differential pressure across nozzle (Pa); ρ = moist air density ($kg\ m^{-3}$); β = d D^{-1}; D = duct hydraulic diameter (0.61 m).

The prediction airflow (Q') was then corrected to standard temperature and barometric conditions by Equation (2) (Heinsohn and Cimbala, 2003).

$$Q_{std} = \frac{Q'}{\left(\frac{P_{std}}{P_b - (P_{ws} \times RH)} \frac{T_{db}}{T_{db,std}} \right)} \quad (2)$$

where, Q_{std} = corrected airflow to standard conditions ($m^3\ s^{-1}$); P_{std} = Standard barometric pressure (101,325 Pa); P_b = actual barometric pressure (Pa); P_{ws} = saturation water vapour partial pressure (Pa); RH = relative humidity of actual conditions (%); T_{db} = actual absolute dry-bulb temperature (K); $T_{db,std}$ = standard absolute dry-bulb temperature conditions (294.25 K)

During transport, the t_{db}/RH sensor and DAQ were stored in a protective case to prevent damage from vibration. The DPT_s and P_b transducers remained installed in the instrumentation cabinet with no supply power. Once on site, previously removed components were installed and all sensors were powered.

2.5 Operational performance

Overall operational performance of MAFT was evaluated during a filter test at a filter DP of 37 Pa using the reference pair of primary and secondary filters to evaluate t_{db}, RH, filter and nozzle DP, and P_b. Data collection was performed using the aforementioned protocol (4 Hz for 15 s) and post-processed to eliminate outliers using Chauvenet's Criterion (ASHRAE Standard, 1976).

2.6 Calibration

The MAFT laboratory was calibrated at the University of Illinois BESS fan test facility (http://bess.illinois.edu/) for airflows ranging from 259 to 1,692 $m^3\ hr^{-1}$ (150 to 1,000 $ft^3\ min^{-1}$) at initial commissioning (January 2017) and after 454 days of operation (April 2018). The filter, nozzle upstream, and exhaust sections were mounted to the wind tunnel outlet. A new primary and secondary filter pair (reference) were installed in the test duct to replicate airflow conditions expected during normal operation. Differential pressures were recorded using DPT_1 to DPT_3, while t_{db} and RH were recorded by BESS. Calibration was performed for increasing (n = 8) and decreasing airflows (n = 8) during the commissioning calibration. The second calibration was performed for increasing (n = 6) and decreasing (n = 5). The calibration equation (Equation (3)) was developed to calibrate the airflow predicted at standard conditions to the reference airflow determined by BESS (Q_{final}). A t-test (α = 0.05; df = 8, DPT_1; df = 13, DPT_2) of the slope assessed whether it was different from unity. At the second calibration, DPT_1 calibration coefficients was compared to the commissioning calibration coefficients; however, DPT_2 was excluded because the original DPT experienced a malfunction and was replaced shortly after commissioning calibration.

$$Q_{final} = b\,Q_{std} + a \quad (3)$$

where, Q_{final} = predicted airflow standard conditions ($m^3\ s^{-1}$); b = slope coefficient; a= intercept coefficient.

Following the initial testing and transportation of the MAFT laboratory, an *in situ* calibration of DPT_1 was performed against a micro-manometer (Model A-302, Dwyer Instruments, Inc.; 0.06 Pa accuracy) to verify for potential drift due to vibration during transportation. Calibration was performed over the full measurement

range (n = 8). Slope and intercept coefficients were compared to the manufacturer's calibration using a t-test (α = 0.05; df = 7).

2.7 Uncertainty analysis

Final predicted airflow standard uncertainty (ΔQ_{final}) was calculated from the standard uncertainty obtained from all key measurement inputs propagated through equations (1), (2), and (3). A zeroth-order uncertainty budget was created for each input: DPT (Table 2), P_b (Table 3), and t_{db} and RH (Table 4) and included the manufacturer's accuracy and long-term stability, quantization error from the 16-bit ADC, and the standard error (SE) from experimental data (SE was removed from the budget as it changes with each experiment (Gates et al., 2009).). All sensors were previously calibrated by the manufacturer according to their specifications and were accompanied with a calibration report. The standard uncertainty associated with nozzle diameter was determined based on one-half the reading resolution set by the manufacturer ($\Delta d = 2.70\times10^{-3}$ m). The standard uncertainty associated with the test duct diameter was calculated as one-half the reading resolution of the measurement device during test duct construction ($\Delta D = 2.10\times10^{-2}$ m). System drift was calculated as a percentage of full scale from the commissioning and second calibration. Drift was determined as the maximum difference of the predicted values for both calibration equations for 100 flows equally spaced between the calibrated airflow range (NIST/SEMATECH, 2013). Combined standard uncertainty associated with MAFT was calculated using data from filter tests completed during the initial months of testing. Selected airflow values ranged from 343 to 1,417 $m^3\ hr^{-1}$ (202 to 834 $ft^3\ min^{-1}$).

Table 2 Uncertainty budget for DPT_1, DPT_2

Source	Value (Pa)	Probability distribution	Divisor	Standard uncertainty (Pa)
Accuracy RSS[a]	2.49, 3.73	Rectangular	$\sqrt{3}$	1.44, 21.55
Long-term stability[b]	0.25, 0.37	Rectangular	$\sqrt{3}$	1.40×10^{-2}, 2.20×10^{-2}
Quantization error[c]	5.70×10^{-3}, 8.50×10^{-3}	Rectangular	$\sqrt{3}$	3.30×10^{-3}, 4.90×10^{-3}
Sensor combined standard uncertainty, ΔDPT_1, ΔDPT_2				1.44, 2.17

Note: [a] Root-Sum-Square (at constant t_{db}), ±1.0% FS DPT_1 (0-248 Pa), DPT_2 (0-373.2 Pa);
[b] Long-term stability, %FS 6 $months^{-1}$;
[c] ±0.5 sensor resolution = (16-bit ADC resolution, 10 V_{DC} reference range = 1.53E-4 V BL^{-1})(sensor sensitivity)$^{-1}$.

Table 3 Uncertainty budget for barometric pressure transducer

Source	Value (Pa)	Probability distribution	Divisor	Standard uncertainty (Pa)
Accuracy RSS[a]	0.34	Rectangular	$\sqrt{3}$	0.20
Long-term stability[b]	0.34	Rectangular	$\sqrt{3}$	0.20
Quantization error[c]	3.20×10^{-3}	Rectangular	$\sqrt{3}$	1.80×10^{-3}
Sensor combined standard uncertainty, ΔP_b				0.28

Note: [a] Root Sum Square (at constant t_{db}), ±1.0% FS (0-137.90 kPa);
[b] Long-term stability, %FS 6 $months^{-1}$;
[c] ±0.5 sensor resolution = (16-bit ADC resolution, 10 V_{DC} reference range = 1.53E-4 V BL^{-1}) (sensor sensitivity)$^{-1}$.

Table 4 Uncertainty budget for temperature and relative humidity sensor

Source	Value (°C, %)	Probability distribution	Divisor	Standard uncertainty (°C, %)
Accuracy RSS[a]	0.2, 1.5	Rectangular	$\sqrt{3}$	0.12, 0.87
Long-term stability[b]	N/A[c], 2.0	Rectangular	$\sqrt{3}$	N/A[c], 1.15
Quantization error[c]	2.70×10^{-3}, 2.30×10^{-3}	Rectangular	$\sqrt{3}$	1.60×10^{-3}, 1.30×10^{-3}
Sensor combined standard uncertainty, Δt_{db}, ΔRH				0.12, 1.44

Note: [a] Manufacturer stated accuracy;
[b] Long term stability, %FS 2 $years^{-1}$;
[c] ±0.5 sensor resolution = (16-bit ADC resolution, 10 V_{DC} reference range = 1.53E-4 V BL^{-1})(sensor sensitivity)$^{-1}$;
[d] Long-term stability is included in accuracy term from manufacturer specifications.

The combined standard uncertainty associated with moist air density (Equation (4)) included the standard uncertainty associated with t_{db}, RH, and P_b measurements.

$$\Delta\rho^2 = \left(\frac{\partial\rho}{\partial t_{db}}\Delta t_{db}\right)^2 + \left(\frac{\partial\rho}{\partial RH}\Delta RH\right)^2 + \left(\frac{\partial\rho}{\partial P_b}\Delta P_b\right)^2 \quad (4)$$

where, $\Delta\rho$ = combined standard uncertainty in moist air density (kg m^{-3}).

The combined standard uncertainty associated with actual airflow prediction (Equation (5)) was obtained by combining the zeroth-order analysis of key inputs and moist air density combined uncertainty.

$$\Delta Q'^2 = \left(\frac{\partial Q'}{\partial d}\Delta d\right)^2 + \left(\frac{\partial Q'}{\partial(Ps_1 - Ps_2)}\Delta(DPT_i)\right)^2 + \left(\frac{\partial Q'}{\partial\rho}\Delta\rho\right)^2 + \left(\frac{\partial Q'}{\partial\beta}\Delta\beta\right)^2 \quad (5)$$

where, $\Delta Q'$= combined standard uncertainty in predicted airflow ($m^3\ s^{-1}$); i = 1 (0 to 248 Pa) or 2 (0 to 373 Pa) for differential pressure transducer.

The combined standard uncertainty associated with airflow prediction at standard conditions (Equation (6)) combined the zeroth-ordered analysis for t_{db}, P_b, and the combined standard uncertainty associated with predicted

airflow.

$$\Delta Q_{std}^2 = \left(\frac{\partial Q_{std}}{\partial Q'}\Delta Q'\right)^2 + \left(\frac{\partial Q_{std}}{\partial P_b}\Delta P_b\right)^2 + \left(\frac{\partial Q_{std}}{\partial t_{db}}\Delta t_{db}\right)^2 \quad (6)$$

where, ΔQ_{std} = combined standard uncertainty airflow at standard conditions ($m^3 s^{-1}$).

The combined standard uncertainty in the final airflow prediction (Equation (7)) was obtained by combining the standard uncertainty in airflow at standard conditions and the RMSE of the calibration.

$$\Delta Q_{final}^2 = \left(\frac{\partial Q_{final}}{\partial Q_{std}}\Delta Q_{std}\right)^2 + RMSE^2 + D^* \quad (7)$$

where, ΔQ_{final} = final airflow prediction combined standard uncertainty ($m^3 s^{-1}$); *RMSE* = root-mean-square error from linear regression (Equation (3); $m^3 s^{-1}$); D^*= long term drift (4.2% $year^{-1}$).

2.8 Verification and validation

Airflow measurements at a 37 Pa (0.15 in. wc) filter DP obtained from the on-site MAFT laboratory and an off-site third-party laboratory (ASHRAE 52.2 certified) were compared for 34 primary and secondary pairs. Filter pairs exhibiting varying levels of dust loading (corresponding to a range of airflows) were sampled from several commercial swine sites in central Iowa across an eight-week period during spring months when ambient relative humidity was low. This timeframe was selected to minimize the effect of moisture on airflow. In addition, all filters were handled according to the manufacturer's recommendations. Filter mass was measured prior to testing with MAFT laboratory and at the off-site third-party laboratory to verify any mass changes possibly incurred during shipping. Selected filter pairs were first tested in MAFT laboratory, and then shipped to the off-site third-party laboratory. Each secondary filter was placed in an individual box with the air entering side facing up and the primary filters were wrapped individually in plastic bags and placed in boxes of six with the air entering side facing up. Filter pair airflows were compared using a linear regression between the off-site third-party laboratory and MAFT laboratory. The residuals were inspected for trends indicating potential airflow measurement bias.

3 Results and discussion

The results presented quantify the operational performance of static DP control, the trailer moist air environment, MAFT laboratory airflow calibration against a reference standard, and overall airflow measurement uncertainty against an off-site third-party laboratory.

3.1 Operational performance

The filter and nozzle DP showed minimal variation with time through the data collection phase of the filter test (Figure 3). The greater SE of the nozzle DP (Table 5) is believed to be caused by increased turbulence upstream of the nozzle. The t_{db} and RH measurements show minimal variation through the 15 s of data collected (Figure 4). No outliers were detected from any measurements over the 15 s of recorded data.

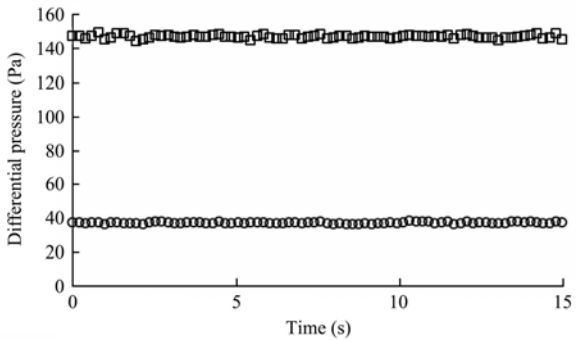

Figure 3 Operational performance data for filter and nozzle differential pressure for the reference filter set

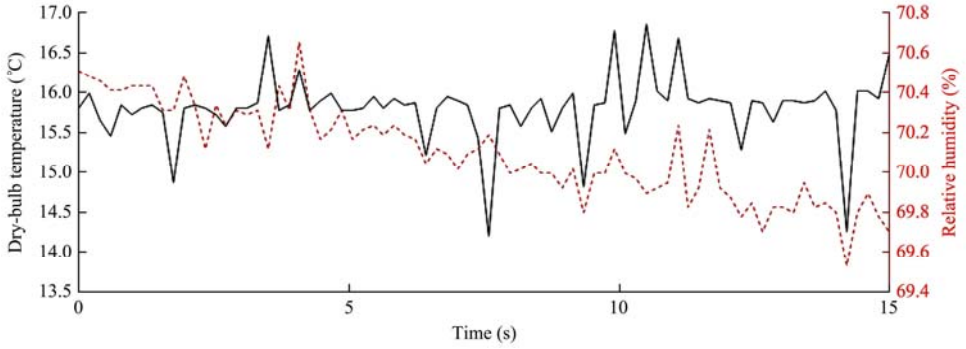

Figure 4 Operational performance data for dry-bulb temperature and relative humidity of moist air running through the duct for the reference filter set

Table 5 Average and SE results from the raw data for a reference filter test

Sensor/Parameter	Average	SE
P_b (Pa)	9.65×10^4	17.0
t_{db} (°C)	15.8	0.1
RH (%)	70.1	0.1
Nozzle DP[a] ($P_{S1} - P_{S2}$; Pa)	146.7	0.1
Filter DP (Pa)	37.1	0.1

Note: [a] Nozzle DP collected from DPT_1.

The circles represent filter DP, and the squares represent the nozzle DP. The nozzle differential pressure was recorded using the DPT_1.

The solid line represents the dry-bulb temperature, and the dashed line represents the relative humidity.

3.2 Calibration

A unique airflow calibration regression was developed for DPT_1 and DPT_2 (Figure 5). Hysteresis was not observed and the coefficient of determination (R^2) exceeded 0.99 for both calibration regressions (Figure 5). The slope was found to be significantly different from unity for DPT_1 (p = 0.0021) and DPT_2 (p = 0.0012) for the commissioning calibration. This suggests that the calibration of MAFT was justified and needed. The offset observed in predicted airflow may be attributed to increased turbulence due to the shorter sections of the test duct and nozzle throat pressure taps. A zero airflow calibration point was not included in the calibration regression to reduce the error in the regression as the offset in DP readings could not be observed at zero airflow.

DPT_1 was calibrated in 2017 (circles) and 2018 (squares); however, DPT_2 experienced a malfunction and was replaced shortly after initial calibration.

The *in situ* calibration of DPT_1 analysis showed that the slope coefficient was not significantly different from the manufacturer's calibration (p = 0.94) and the intercept coefficient was significantly different (p = 0.0002). The change in the intercept coefficient over time was minimal (0.011 to 0.006 Pa), but the differences in the calibration set-up could have been a contributing factor. Both DPTs 1 and 2 will need to be calibrated frequently in the future to maintain an accurate intercept coefficient.

3.3 Uncertainty analysis

Relative expanded uncertainty (coverage factor = 2; ~95% confidence level) ranged from 5% at 343 $m^3\ hr^{-1}$ and 1.5% at 1,417 $m^3\ hr^{-1}$. The segmentation observed in the relative and absolute expanded uncertainties (Figure 6) is a result of the two unique DPTs used in MAFT. For future work, a higher accuracy (0.04% FS accuracy; Model 267, Setra, Inc.) DPT for the 0 to 373.2 Pa range might reduce the increase in measurement uncertainty within the transition range of the DPTs.

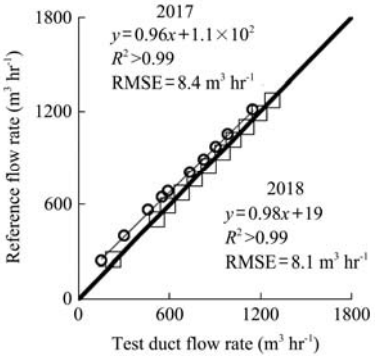

(a) DPT_1

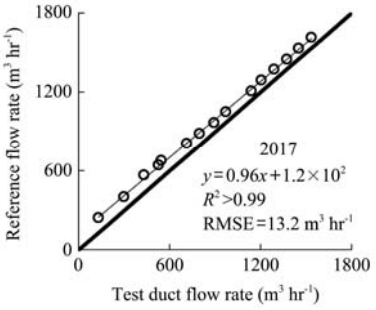

(b) DPT_2

Figure 5 Calibration curve for DPT_1 (a) and DPT_2 (b) with linear regression between the test duct airflow (x-axis) and the calibration reference airflow (y-axis)

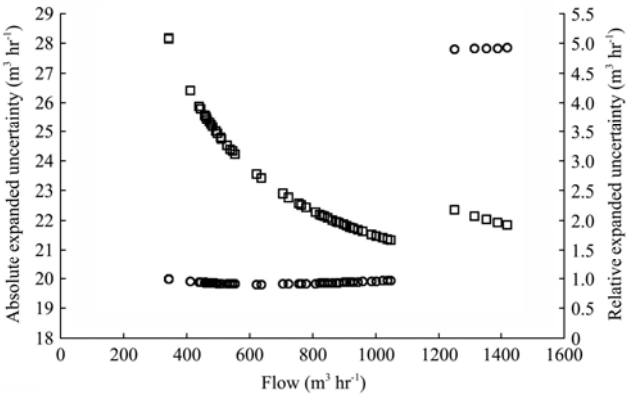

Figure 6 Absolute and relative uncertainty associated with airflow measurements from MAFT

The circles represent absolute uncertainty, and the squares represent relative uncertainty. For airflows less than 1,080 $m^3\ hr^{-1}$ the average of both DPTs was used, for airflows greater than 1,080 $m^3\ hr^{-1}$ the DPT_2 was used.

3.4 Verification and validation

A total of 34 filter pairs (primary and secondary

filters) were tested for the verification and validation of MAFT at airflow rates from 576 to 1,440 $m^3 hr^{-1}$ (320 to 830 $ft^3 min^{-1}$). No significant difference ($p < 0.001$) in prior and post shipping mass were noted for the filters pairs tested. Figure 7(a) shows both the off-site third-party laboratory and MAFT laboratory airflow predictions.

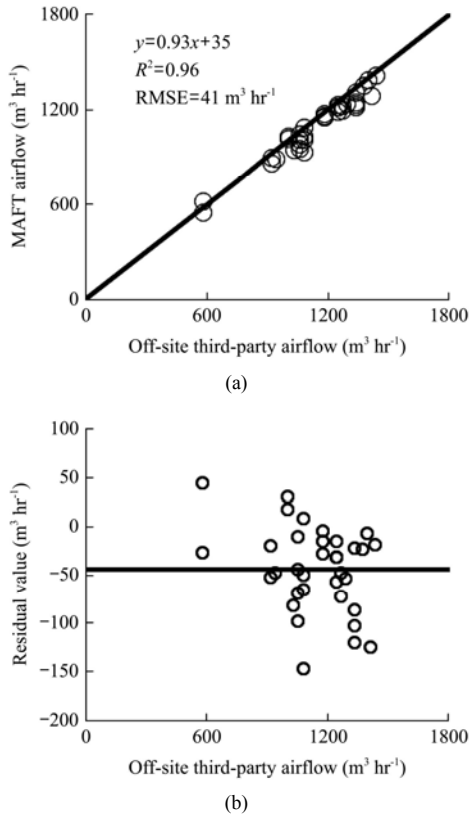

(a)

(b)

Figure 7 a) Comparison of all 34 filters tested between MAFT and the off-site third-party laboratory; b) Linear relationship between the airflow prediction from the off-site third-party laboratory (x-axis) and the residual between MAFT and the off-site third-party laboratory's airflow prediction (y-axis). The solid line represents the average residual value

Further analysis of the residual values between MAFT and the off-site third-party laboratory show a slight negative bias on the average of MAFT prediction residuals, –44 $m^3 hr^{-1}$ (–26 $ft^3 min^{-1}$) or –4% (Figure 7). There are multiple factors that could have caused the bias in the residuals, such as variations in testing protocols and sensor accuracy. It is difficult to match the filter DP during testing across multiple laboratories. Shipping filters could have also played a role in the observed bias as dust settling in the media could have occurred during shipping and affected airflow. For future comparisons and testing collaborations with a specific off-site third-party laboratory, the bias can be accounted for in the data analysis. A bias would need to be determined for each new off-site third-party laboratory used in the future research, as 5% variance between labs is common.

4 Conclusions

A custom mobile air filter testing (MAFT) laboratory capable of providing airflows from 259 to 1,692 $m^3 hr^{-1}$ (150 to 1,000 $ft^3 min^{-1}$) was designed, constructed, calibrated, and validated. The test duct was mounted in an enclosed trailer for easy transportation from site to site. The test duct was built using clear acrylic plastic and utilized a long radius nozzle to determine airflow. Relative standard uncertainty was calculated to range from 5% to 1.5% for airflows ranging from 343 to 1,417 $m^3 hr^{-1}$ (202 to 834 $ft^3 min^{-1}$), respectively. The mobile aspect of this laboratory makes it ideal for filter resistance testing on breeding-gestation-farrowing facilities for cost effective testing of a representative sample for the site.

The MAFT laboratory conformed to the ASHRAE 52.2 standard in numerous ways. Mainly in the test duct cross sectional dimensions, airflow measurement, and location of static pressure locations. The overall length, while based on the ASHRAE 52.2 standard, was not the exact dimensions specified in the standard. Static pressure measurement was accomplished using static only pitot tubes, whereas the standard called for static pressure taps. The construction of MAFT laboratory did not allow for static pressure taps to be employed. Overall MAFT was designed for a unique filter resistance application and conformed to the ASHRAE 52.2 standard as applicable.

5 Practical applications

For animal housing applications, filter end-of-life can be determined based on a minimum allowed airflow at the design pressure differential, to prevent the onset of heat stress conditions inside the building due to lowered ventilation rates. By testing on-site, filter life span can be maximized by accurately measuring filter airflow to determine which filters warrant replacement, compared to solely replacing filters after fixed durations of use. This allows a producer to make targeted filter replacement decisions to replace the filters that absolutely need to be replaced. This can substantially reduce the costs of

frequent filter changes and reduce the disease transmission risk associated with changing filters.

An explicit biosecurity plan must be in place to safely accomplish site to site testing. Components of such a plan was included throughout the design and construction of the laboratory. The intake filters on the blower will prevent the contamination of the filters being tested and can easily be replaced between sites, the use of a test primary or secondary filter will be limited to a specific site or group of sites based on the producer's preferences, and the interior of the enclosed trailer and test duct allow for easy cleaning and disinfection. The outside of the trailer and the truck used to pull the trailer must be washed and disinfected as well between sites. These areas and tasks are fundamental for preventing the spread of disease from site to site from filter testing using MAFT. On-site filter resistance testing with MAFT is preferable, in our opinion, as it has an acceptable measurement uncertainty and addresses the biosecurity and logistical concerns.

Acknowledgments

This work was supported by in-kind donations from Iowa Select Farms. The authors would like to thank Blake Fonken for assistance during the construction and validation of the laboratory. The authors would like to thank Dr. Dan Andersen for technical assistance in the preparation of this manuscript.

References

Albright, L. D. 1990. *Environment Control for Animals and Plants*. St. Joseph, MI: American Society of Agricultural Engineers.

Alonso, C., P. R. Davies, D. D. Polson, S. A. Dee, and W. F. Lazarus. 2013a. Financial implications of installing air filtration systems to prevent PRRSV infection in large sow herds. *Preventive Veterinary Medicine*, 111(3-4): 268–277.

Alonso, C., M. P. Murtaugh, S. A. Dee, and P. R. Davies. 2013b. Epidemiological study of air filtration systems for preventing PRRSV infection in large sow herds. *Preventive Veterinary Medicine*, 112(1): 109–117.

ASHRAE Standard. 1976. ASHRAE 41.5-75. Standard measurement guide- Engineering analysis of experimental data. Atlanta, GA.: American Society of Heating Refrigerating and Air-Conditioning Engineers.

ASHRAE Standard. 2012. ANSI/ASGHRAE Standard 52.2-2012. Method of testing general ventilation air-cleaning devices for removal efficiency by particle size. Atlanta, GA.: ASHRAE.

ASHRAE. 2013. *ASHRAE Handbook Vol. Fundamentals*. Atlanta, GA: ASHRAE.

Dee, S. A., J. Deen, J. P. Cano, L. Batista, and C. Pijoan. 2006. Further evaluation of alternative air-filtration systems for reducing the transmission of porcine reproductive and respiratory syndrome virus by aerosol. *Canadian Journal of Veterinary Research*, 70(3): 168.

Dee, S., S. Otake, and J. Deen. 2010. Use of a production region model to assess the efficacy of various air filtration systems for preventing airborne transmission of porcine reproductive and respiratory syndrome virus and Mycoplasma hyopneumoniae: results from a 2-year study. *Virus Research*, 154(1): 177–184.

Gates, R. S., K. D. Casey, H. Xin, and R. T. Burns. 2009. Building emissions uncertainty estimates. *Transactions of the ASABE*, 52(4): 1345–1351.

Heinsohn, R. J., and J. M. Cimbala. 2003. *Indoor air quality engineering: environmental health and control of indoor pollutants*. Boca Raton, FL : CRC Press.

Holtkamp, D., J. Kliiebenstein, E. Neumann, J. J. Zimmerman, H. Rotto, Y. Tiffany, and C. Haley. 2013. Assessment of the economic impact of porcine reproductive and respiratory syndrome virus on United States pork producers. *Journal of Swine Health and Production*, 21(2): 72.

Jadhav, H. T., Hoff, S. J., Harmon, J. D., Alvarez, I., Andersen, D. S., & Passe, U. 2018. Swine Finishing Room Air Infiltration: Part 1. Quantification and Prediction. *Applied Engineering in Agriculture*, *34*(2), 413–424.

McQuiston, F. C., J. D. Parker, and J. D. Spitler. 2005. *Heating, Ventilating, and Air Conditioning: Analysis and Design*. 6th ed. Hoboken, NJ: John Wiley & Sons, INC.

Midwest Plan Service. 2010. *Structures and environment handbook MWPS-1-TSM*. Ames, IA: Iowa State University.

NIST/SEMATECH. 2013. e-Handbook of Statistical Methods. Available at: https://www.itl.nist.gov/div898/handbook/mpc/section4/mpc46.htm#drift. Accessed May 1, 2018.

Ramirez, B. C., S. J. Hoff, , J. D. Harmon, and J. P. Stinn. 2016. Thermal environment performance and uniformity assessment for a novel swine breeding and gestation facility. 1–9. Available at: https://doi.org/10.13031/aim.20162454577. Accessed July 17, 2016.

Ramirez, A., and P. Zaabel. 2012. Swine Biological Risk Management. The Center for Food Security and Public Health: Iowa State University. Available at: http://www.cfsph.iastate.edu/pdf/swine-biological-risk-management. Retrieved August 20, 2017.

Thornton, P. K. 2010. Livestock production: recent trends, future prospects. *Philosophical Transactions of the Royal Society B:*

Biological Sciences, 365(1554): 2853–2867.

University of Illinois. 2012. University of Illinois Department of Agricultural and Biological Engineering Bioenvironmental and Structural Systems Lab Final Report No. 12790. Available at: http://bess.illinois.edu/pdf/12790.pdf. Accessed October 15, 2017.

Nomenclature

a	= intercept coefficient
β	= d D^{-1}
b	= slope coefficient
C_d	= discharge coefficient (0.98)
D	= duct hydraulic diameter (0.61 m)
D^*	= long term drift (%)
d	= nozzle diameter (0.15 m)
i	= differential pressure transducer 1 or 2
P_{Sa}	= static pressure measurement location prior to filters
P_{Sb}	= static pressure measurement location post filters
Ps_1	= static pressure measurement location prior to the nozzle
Ps_2	= static pressure measurement location in the nozzle throat
P_b	= actual barometric pressure (Pa)
P_{std}	= Standard barometric pressure (101,325 Pa)
P_{ws}	= saturation water vapour partial pressure (Pa)
Q_{final}	= predicted airflow standard conditions ($m^3 s^{-1}$)
Q_{std}	= corrected airflow to standard conditions ($m^3 s^{-1}$)
Q'	= predicted airflow ($m^3 s^{-1}$)
RH	= relative humidity of actual conditions (%)
$RMSE$	= root mean square error of the calibration
ρ	= moist air density (kg m^{-3})
T_{db}	= actual absolute dry-bulb temperature (K)
$T_{db\ std}$	= standard absolute dry-bulb temperature conditions (294.25 K)
ΔD	= standard uncertainty of the duct hydraulic diameter
Δd	= standard uncertainty of the nozzle diameter
ΔDPT_1	= differential pressure transducer 1 zeroth-order standard uncertainty
ΔDPT_2	= differential pressure transducer 2 zeroth-order standard uncertainty
ΔP_b	= barometric pressure transducer zeroth-order standard uncertainty
ΔRH	= relative humidity zeroth-order standard uncertainty
$\Delta\rho$	= combined standard uncertainty in moist air density (kg m^{-3})
Δt_{db}	= dry-bulb temperature zeroth-order standard uncertainty
ΔQ_{final}	= combined standard uncertainty of the final airflow prediction
ΔQ_{std}	= combined standard uncertainty of airflow at standard conditions
$\Delta Q'$	= combined standard uncertainty of predicted airflow ($m^3 s^{-1}$)